IEEE Access
Multidisciplinary | Rapid Review | Open Access Journal

Received February 24, 2020, accepted March 11, 2020, date of publication March 19, 2020, date of current version March 30, 2020.

Digital Object Identifier 10.1109/ACCESS.2020.2982015

Research on Simulation, Experiment and Evaluation Method of Different Ratio Gd Doped $AgSnO_2$ Contact Material

YING ZHANG[1], JINGQIN WANG[1], GUANGZHI ZHANG[2], AND ZHIZHOU BAO[3]

[1]State Key Laboratory of Reliability and Intelligence of Electrical Equipment, Electrical Engineering Department, Hebei University of Technology, Tianjin 300130, China
[2]Shanghai Liangxin Electrical Company, Ltd., Shanghai 200120, China
[3]Zhejiang People Electric Appliance Company, Ltd., Wenzhou 325604, China

Corresponding author: Jingqin Wang (jqwang@hebut.edu.cn)

This work was supported by the National Natural Science Foundation of China under Contract 51777057.

ABSTRACT $AgSnO_2$ electrical contact material with greenery and good performance has the most potential to replace the toxic AgCdO. However, SnO_2 in $AgSnO_2$ contact material is a kind of semiconductor with wide band gap, which is almost insulated and has high hardness, resulting in the increase of contact resistance and temperature rise, and easy to form microcracks. First principle based on density functional theory are used to simulate three doping ratios (8.3%, 12.5%, 16.7%) of rare earth element Gd doped SnO_2. The simulation results show that when the doping ratio is 12.5%, electrical performance is the best. As the doping ratio increases, the smaller the hardness, the higher the probability of microcracks. To more objectively obtain the doping ratio with the best comprehensive performance, the comprehensive evaluation model of Technique for Order Preference by Similarity to Ideal Solution with entropy weight is adopted to evaluate, and the performance with doping ratio of 12.5% is the best. Finally, it is verified by experiments. Different ratio of Gd doped SnO_2 powders are prepared by the sol-gel method, and the X-ray diffraction test proves that the sol-gel method can realize the substitution doped model established by simulation. The doped $AgSnO_2$ is prepared by powder metallurgy method, and its electrical performance and hardness are measured. The theory and experiment can be well matched, which proves the feasibility and credibility of simulation. It provides a new idea and scientific reference for the research on doping to improve the properties of $AgSnO_2$ contact material.

INDEX TERMS $AgSnO_2$ contact material, doping, first principle, comprehensive evaluation method.

I. INTRODUCTION

AgCdO contact material has the advantages of resistance to arc erosion and fusion welding, low contact resistance, stability, and the applied current ranges from tens to thousands, which was once called ''universal contact'' [1], [2]. In 2003, the European Union issued ''the restriction of the use of certain hazardous substances in electrical and electronic equipment'' (RoHS Directive) to ban the use of six hazardous substances, including Cd, in electrical equipment from July 2006. Although the Cd and Cd compounds in electrical contacts are exempted in the ''RoHS Directive,'' it is reapproved every four years. In 2019, the European Union revised the regulations for the content of Cd in the ''RoHS Directive''. According to the revised directive, it is clear that Cd and its compounds in electrical contacts are exempted in most applications until July 21, 2021, a few special applications can be exempted to the latest on July 21, 2024 [3], [4]. Due to the requirements of environmental protection, and AgCdO materials are increasingly difficult to meet the performance of electrical switches for contact materials such as high reliability and long life [5]. It is urgent for us to find a new contact material to replace AgCdO.

After long time research, $AgSnO_2$ is an environmentally friendly contact material that is comparable to AgCdO and most potential to replace AgCdO [6], [7]. However, it is found in the application that the conductivity of $AgSnO_2$ contact material is worse than AgCdO under the same conditions. Because SnO_2 is a wide band gap semiconductor material, Under the continuous action of arc, SnO_2 with

The associate editor coordinating the review of this manuscript and approving it for publication was Chong Leong Gan.

This work is licensed under a Creative Commons Attribution 4.0 License. For more information, see https://creativecommons.org/licenses/by/4.0/

high decomposition temperature and non-conductivity is easy to accumulate on the contact surface, which increases the contact resistance and affects the electrical life. Moreover, the hardness of SnO_2 is high, making the material brittle, cracks are easy to form, and the repeated deformation ability is poor, reducing electrical wear resistance and life [8].

Small amount of dopant has always been an important research direction for improving the performance of $AgSnO_2$ contact materials at home and abroad, especially the research of rare earth element doped $AgSnO_2$ [9]–[12]. The experimental research results show that the rare earth oxide has high melting point and good stability. $AgSnO_2$ contact material with small amount of doped rare earth element can ensure stability at higher temperatures, thereby improving the stability of the contact. Rare earth atoms can refine the grains, improving properties of $AgSnO_2$ contact materials [13]. Therefore, more and more attention has been paid to the doping modification of $AgSnO_2$ contact materials by rare earth element, and more and more research results have been achieved in recent years.

Although there are more and more studies on doping to improve the $AgSnO_2$ contact material, most of them focus on experimental research, and the selection of doped content is only based on experience. After preparation of samples, a series of related experiments are carried out to compare, so the conclusion has contingency and limitation. Even though it has been found in experiment that doping with rare earth elements can improve the electrical and mechanical properties of $AgSnO_2$ contact materials, the modification mechanism of rare earth doping is still unclear. Therefore, the current research on $AgSnO_2$ contact materials is urgently needed to seek effective microstructure design and performance prediction to improve its conductivity, hardness and cracks to increase its life.

The micro scale is mainly for the simulation of electronic structures. The main method is the first principle based on density functional theory. The first principle method can simulate a system with a periodic structure and can solve the ground electronic structure and properties of the system without relying on any empirical parameters. It is an important means to design materials.

At present, most of theoretical researches focus on the influence of doping on the electrical properties of materials, and few studies on mechanical properties [14]. Moreover, most of the doping ratio is selected through experience, resulting in high cost of manpower, material and financial resources. This paper is based on the first principle of density functional theory, three different ratio of Gd doped SnO_2 are selected. The electrical and mechanical properties are studied to find the doping ratio with the best comprehensive performance.

When we study the doping ratio with the best comprehensive performance, sometimes all performance parameters obtained under a certain doping ratio are not the best at the same time. In order to make a more scientific and reasonable choice, a comprehensive performance evaluation system is extremely important. In this paper, a comprehensive evaluation system of Technique for Order Preference by Similarity to Ideal Solution (TOPSIS) with entropy weight is constructed, in which the weight of indicators is determined by the entropy method, so that human interference factors can be effectively eliminate. The conclusion is based on the original data and makes the final evaluation result more objective and justice [15]. Finally, TOPSIS method is used for quantitative analysis, evaluation and comparison, drawing the final conclusion.

II. SIMULATION

A. BASIC PRINCIPLES

The calculation in this paper uses the first principle method based on density functional theory, which is completed by the CASTEP module in Software Studio 17.2. The periodic boundary conditions are adopted in the calculation process. The exchange correlation potential energy is optimization using the Perdew Burke Ernzerhof (PBE) method under Generalized Gradient Approximation (GGA) and the elastic constant using CA-PZ under Local Density Approximation (LDA) method. The crystal wave function is expanded by plane wave basis vector, and the interaction potential between the real ion and valence electron is described by Ultra Soft Pseudopotential (USPP) [16].

The idea of Local Density Approximation is to approximate the exchange correlation energy to a quantity that is only related to the electron density at a certain point, and the value of the exchange correlation energy is equal to the exchange correlation energy of a uniform field with the same charge density. The calculation of elastic constant has achieved good results [17].

Generalized Gradient Approximation introduces the electron density gradient term, solving the problem that the exchange correlation function changes when the electron density changes greatly. The calculation results such as structure optimization and experimental results are in good agreement [18].

Ultra Soft Pseudopotential introduces a generalized orthogonal normalization condition, which makes the wave function smoother and requires fewer plane wave basis functions, reducing the amount of calculation.

The valence electron configuration considered in the calculation is: O $2s^2 2p^4$, Sn $5s^2 5p^2$, Gd $4f^7 5p^6 5d^1 6s^2$.

B. CONSTRUCTION OF CRYSTAL CELL

SnO_2 is a tetragonal rutile structure with a space group of 136, as shown in Fig. 1(a). The red sphere represents O atom and the gray sphere represents Sn atom. The SnO_2 unit cell contains two Sn atoms and four O atoms. The Sn atoms occupy the apex and body center of the lattice, and each Sn atom is adjacent to 6 O atoms, and each O atom is adjacent to 3 Sn atoms, with a coordination number of 6:3. The lattice constants are: a = b = 0.4737nm, c = 0.3816nm, $\alpha = \beta = \gamma = 90^o$ [19], [20]. The supercell models are used in the

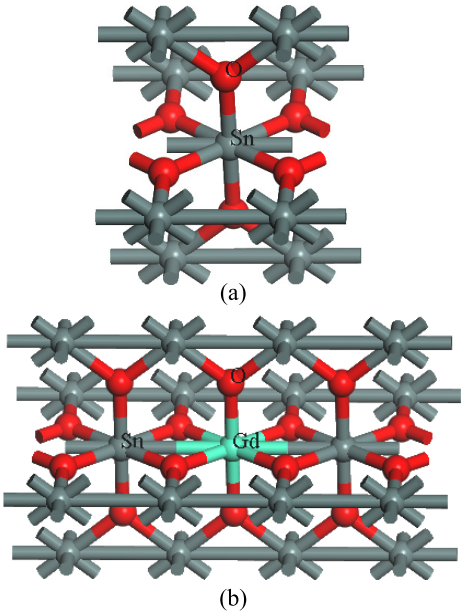

FIGURE 1. Cell model (a) SnO_2 (b) 16.7%-Gd doped SnO_2.

TABLE 1. Doping ratio and supercell correspondence.

Supercell	Doping Ratio
1×1×3	16.7%
1×2×2	12.5%
1×2×3	8.3%

calculation, with 16.7% doping as an example. The SnO_2 is established as a $1 \times 1 \times 3$ supercell, and a Sn atom in the SnO_2 supercell model is replaced with a doped atom Gd. As shown in Fig. 1(b), the green sphere represents doped Gd atoms. The supercell models corresponding to other doping ratios are shown in Table 1.

III. ANALYSIS OF ELECTRICAL AND MECHANICAL PROPERTIES

A. STABILITY ANALYSIS AFTER OPTIMIZATION

Firstly, SnO_2 and Gd doped SnO_2 are optimized. The atomic coordinates and cell parameters are adjusted through iterative processes to minimize the energy, find the most stable point of the structure, and make the structure closest to the real situation, so as to ensure the reliability and accuracy of the crystal electronic structure analysis, energy calculation and elastic constants calculation.

Enthalpy change is the energy released or absorbed by different types of atoms from elementary states to compounds, and it indicates how easy or difficult a compound is to form. Equation (1) is the enthalpy change [12]–[21].

$$\Delta H = \frac{E_{tot}^{AB} - N_A E_{solid}^{A} - N_B E_{solid}^{B}}{N_A + N_B} \quad (1)$$

E_{tot}^{AB} is the total energy of the crystal,
E_{solid}^{A} is the average energy of the solid atoms A
E_{solid}^{B} is the average energy of the solid atoms B,
N_A and N_B are the number of A and B atom, respectively.

When the enthalpy change is negative, the larger the absolute value is, the more stable the intermetallic compound is.

The optimized lattice constant, volume and enthalpy are shown in Table 2.

TABLE 2. Optimized cell parameters.

Doping Ratio	Lattice Constant a/Å	b/Å	c/Å	Volume /Å^3	Enthalpy /eV
16.7%	4.953	4.953	3.310	81.929	-2.3
12.5%	4.939	4.954	3.302	80.790	-2.7
8.3%	4.927	4.926	3.305	80.208	-3.8
0	4.737	4.737	3.186	71.508	-0.5

The enthalpy changes of SnO_2 and Gd doped SnO_2 are all negative, indicating that the structures are stable. After doped Gd with different ratio, the volume increases to different degrees and the doped models are more stable.

B. ENERGY BAND AND DENSITY OF STATES

When performing first principle calculations, several K points with high symmetry in the Brillouin region of three-dimensional space are connected to form a one-dimensional path. There are different electron energy bands of multiple electrons on the K path. A two-dimensional energy band is obtained from K path and energy.

Then, the energy calculation of the optimized models is calculated, and the energy band is shown in Fig. 2. (a) is the energy band of SnO_2. (b), (c), and (d) are the energy band of Gd doped SnO_2, with the doping ratios of 16.7%, 12.5% and 8.3%, respectively.

The energy value at 0 eV indicates the position of the Fermi level. Above 0eV is the conduction band, and below 0eV is the valence band.

Density of states is a visualization of the energy band, which is more intuitive than the energy band. It represents the distribution of electrons at different energy values, that is, the number of electronic states in the unit energy interval of the system. The energy of different atomic orbits is different, so the density of states can be used to characterize the arrangement of electrons outside the nucleus and the interaction between atoms and atoms.

Total Density of States (TDOS) represents the energy distribution state of all electrons in the system. Partial Density of States (PDOS) represents the bonding of electrons in different orbits.

Fig. 3 shows the density of states obtained by optimizing the supercell models. (a) is the density of states of SnO_2.

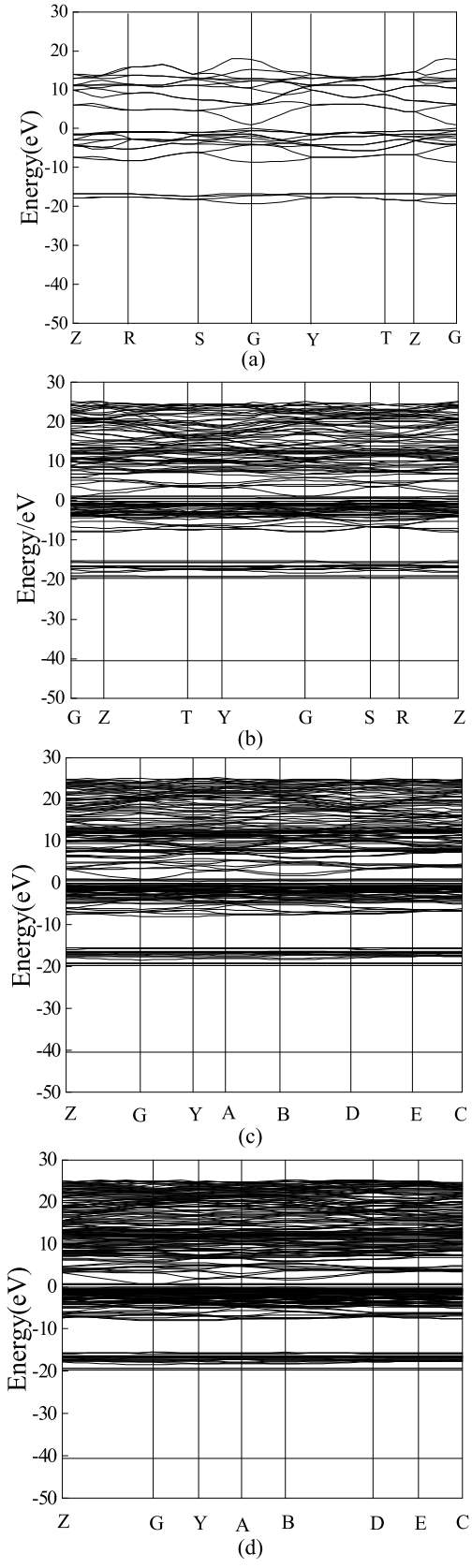

FIGURE 2. Band structure (a) SnO_2 b) 16.7%-Gd doped SnO_2 (c) 12.5%-Gd doped SnO_2 (d) 8.3%-Gd doped SnO_2.

(b), (c), and (d) are the density of states of Gd doped SnO_2, with the doping ratios of 16.7%, 12.5% and 8.3%, respectively.

After several different doping ratios, the bands gap decreases, and the conduction and valence band become dense. The number of electrons transitioning from the valence band to the conduction band increases, which can improve the conductivity, and the fluctuation between the bands becomes gentle, indicating that the electron locality is enhanced after doping.

The width of the bottom band can reflect the ability of the electron to participate in bonding: if the width of bottom band is large, the atomic orbital expands strongly, and the ability of electron to participate in bonding is large [23]. After doping, the width of the bottom band gradually increases, and the bonding ability of the hybrid orbitals is stronger than that of the unhybridized atomic orbitals. Therefore, the ability of electrons to participate in bonding is improved after doped Gd.

The Partial Density of States can more clearly show the specific situation of each electron orbit of the atom.

Fig. 3 (a) shows the density of states of SnO_2, the valence band part at -20eV to -15eV is mainly the 2s state contribution of O, and in the valence band part of -10eV to 0eV, the density of states at the top of the valence band is mainly contributed by the 2p state of O. In the conduction band from 0eV to 20eV, the density of states at the bottom of the conduction band is mainly contributed by the 5s and 5p states of Sn.

From the density of states of SnO_2 doped with Gd in different ratio in Fig. 3 (b)-(d), we can be see that the new peaks in the region of -40eV are mainly caused by the 6s state of Gd, and the contribution of the energy level in the deep orbit to the conductivity is small, so it is not discussed. In the range of -20eV to -15eV, it is contributed by 5p state of Gd atom and 2S state of O atom. Moreover, the peak value of the s orbital of the O atom decreases after doping, indicating that the O atom has a bonding effect on the Gd atom. The valence bands all cross the Fermi level, which indicates that the doping of rare earth element Gd results in stronger interactions between different atoms, the distance from the excitation from the valence band to the conduction band decreases, and the required energy decreases, and the conductivity of SnO_2 is enhanced. Near the Fermi level, in addition to the contributions of the 2p state of O, the 5s and 5p states of Sn, the contribution of the 4f state of Gd, and the position change tends to gradually move in the direction of the conduction band, reducing the energy gap of SnO_2. It is found on the ordinate that the contribution of the 4f state of Gd to the vicinity of the Fermi level is relatively large. The contribution of the rare earth element Gd to the density of states near the Fermi level proves the contribution of the rare earth element Gd to the conductivity. In the conduction band, the d orbit of Gd atom and the s and p orbit of Sn appear hybridization.

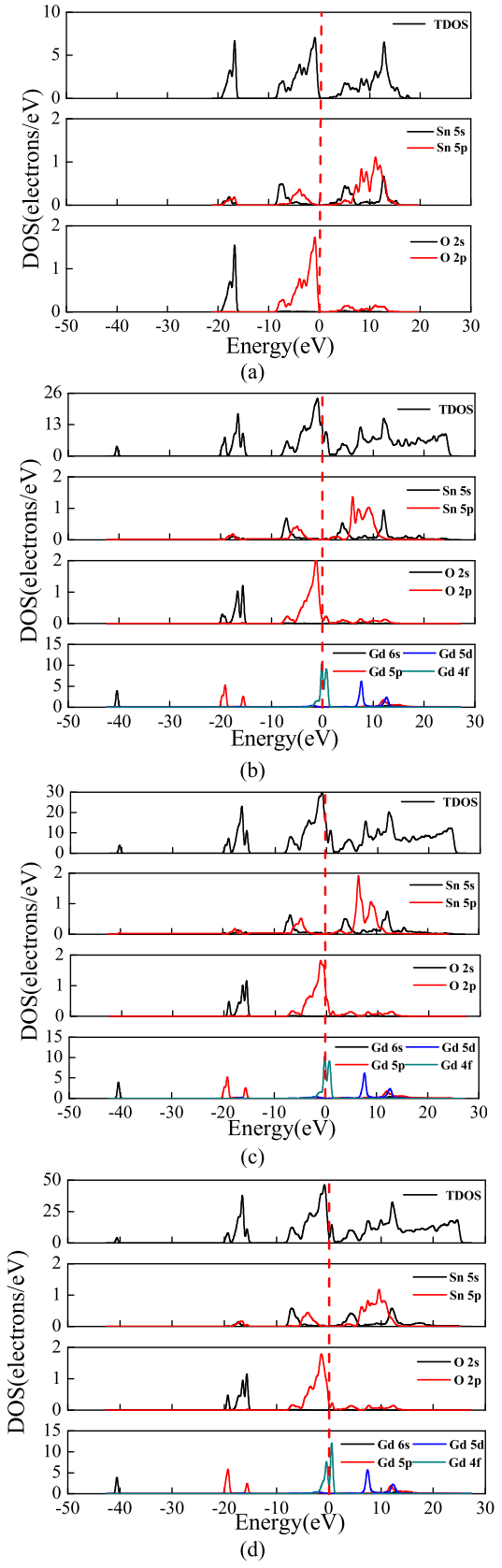

FIGURE 3. Density of states (a) SnO_2 b) 16.7%-Gd doped SnO_2 (c) 12.5%-Gd doped SnO_2 (d) 8.3%-Gd doped SnO_2.

C. RELATIVE CONDUCTIVITY

To further compare the conductivity of the three doping ratios, according to the theory of semiconductor physics, we can know that the conductivity of materials can be characterized by the conductivity δ_i [24].

$$\delta_i = n_i q \mu_i \tag{2}$$

where q is the constant of electron charge, n_i is the electron concentration and μ_i is the electron mobility.

At low temperatures, semiconductor scattering is dominated by ionized impurities. After doped Gd atoms, they form a Coulomb potential field. The Coulomb potential field locally destroys the periodic potential field near the impurity, which is an additional potential field of electron scattering. When the electrons move near the ionized impurities, the electrons are scattered due to the Coulomb potential field. Because the effect of ionizing impurity scattering is related to the doping concentration. According to semiconductor theory, the carrier scattering probability (P_i) of the ionized impurity with doping concentration (N_i) and the temperature (T) is

$$P_i \propto N_i \cdot T^{-3/2} \tag{3}$$

Because the mean free time (τ_i) is the inverse of the scattering probability, the mean free time of ionizing impurities is

$$\tau_i \propto N_i^{-1} \cdot T^{3/2} \tag{4}$$

The relationship between the electron mobility (μ_i) and the mean free time and the electron effective mass (m_e^*) at a certain temperature could be expressed as

$$\mu_i = \frac{q \cdot \tau_i}{m_e^*} \tag{5}$$

Therefore

$$\mu_i \propto \frac{q}{m_e^* \cdot N_i} \tag{6}$$

Electron effective mass is written by

$$m_e^* = \frac{h^2}{4\pi^2 \frac{d^2E}{dk^2}} \tag{7}$$

Among them, h is the Planck constant, k is the wave vector, and E is the electron energy at the wave vector. Therefore, the conductivity is inversely proportional to the doping concentration and the electron effective mass, and is proportional to the electron concentration. The relationship is as follows.

$$\delta_i \propto \frac{n_i}{m_e^* . N_i} \tag{8}$$

According to the actual situation modeled in this paper, to compare the effects of Gd atoms with different doping ratios on the conductivity, we only need to simply compare them to get the relative conductivity, as shown in (9).

$$\frac{\delta_i}{\delta_j} = \frac{n_i \cdot m_{ej}^* \cdot N_j}{n_j \cdot m_{ei}^* \cdot N_i} \tag{9}$$

The electron concentration can be obtained by integrating the density of states by Origin software, and the electron effective mass can be obtained by secondary derivative of the energy band. The calculated data are shown in Table 3.

TABLE 3. Relative conductivity.

Ratio	16.7%	12.5%	8.3%
Two Derivation	312.4	274.8	200.9
Electron Effective Mass/10^{-32}kg	3.6	4.1	5.6
Electron Number	9.2	8.6	6.6
Electron Concentration /10^{21}cm^{-3}	11.3	10.7	8.2
Relative Conductivity	0.91	1	0.84

When the doping ratio is 12.5%, the conductivity is the best. The second is 16.7%.

D. ELASTIC CONSTANT

To calculate the mechanical properties of SnO_2 and Gd doped SnO_2, the famous VRH approximation is used. In general, the bulk modulus (B) and shear modulus (G) of the crystal are related to the elastic constant $C_{ij}(i, j = 1 \sim 6)$. There are commonly two different approaches to approximate calculations. Among them, the Voigt approximation considers the strain to be uniformly distributed, and the Reuss approximation considers the stress to be uniformly distributed. The condition that the Voigt and the Reuss established is that the target polycrystal must be composed of isotropic crystals, whereas the actual materials are generally polycrystals [25], [26]. Voigt and Reuss models can calculate the maximum and minimum values of bulk modulus (B_V and B_R) and shear modulus (G_V and G_R) respectively. Hill uses the arithmetic mean of Voigt and Reuss models as theoretical values, that is, VRH approximation. The bulk modulus and the shear modulus are closer to the experimental values, and their Equations are as follows [27].

$$B_{\mathrm{V}} = \frac{1}{9}(2\,C_{11} + C_{33}) + \frac{2}{9}(2\,C_{13} + C_{12}) \tag{10}$$

$$B_{\mathrm{R}} = \frac{(C_{11} + C_{12})\,C_{33} - 2\,C_{13}^2}{C_{11} + C_{12} + 2\,C_{33} - 4\,C_{13}} \tag{11}$$

$$G_{\mathrm{V}} = \frac{1}{15}(2\,C_{11} + C_{33} - C_{12} - 2\,C_{13}) + \frac{1}{5}(2\,C_{44} + C_{66}) \tag{12}$$

$$G_{\mathrm{R}} = 15\left(\frac{18\,B_{\mathrm{V}}}{(C_{11}+C_{12})\,C_{33}-2C_{13}^2} + \frac{6}{C_{13}-C_{12}} + \frac{6}{C_{44}} + \frac{3}{C_{66}}\right)^{-1} \tag{13}$$

$$B = (B_{\mathrm{V}} + B_{\mathrm{R}})/2 \quad G = (G_{\mathrm{V}} + G_{\mathrm{R}})/2 \tag{14}$$

Due to the anisotropy of its own structure, solid materials also have anisotropy in their elastic properties. To describe the degree of elastic anisotropy of crystals, Ranganathan and Martin [28] introduced the universal elastic anisotropy index (A^U) for all crystals:

$$A^{\mathrm{U}} = 5\frac{G_{\mathrm{V}} + B_{\mathrm{V}}}{G_{\mathrm{R}} + B_{\mathrm{R}}} - 6 \tag{15}$$

The hardness can be determined by the compound microscope designed by chemical bonding. At present, bonding resistance, bonding strength and electronegativity models can be used to evaluate the hardness of known crystals. More importantly, the hardness prediction based on the designed crystal structure becomes feasible in these models. Based on these, the dataset of Chen *et al.* [29] is fitted, and a revised Equation for hardness is given [30].

$$H_V = 0.92K^{1.137}G^{0.708} \tag{16}$$

Among them, $k = G/B$.

The Equation well agrees with the experimental values when hardness is larger than 5 GPa.

TABLE 4. Elastic constant.

Ratio	16.7%	12.5%	8.3%	0
B/GPa	98.26	97.85	99.55	72.6
G/GPa	72.75	74.71	78.61	82.2
HV/GPa	13.60	14.35	15.46	24.03
A^{U}	0.99	0.89	0.84	1.393
G/B	0.740	0.764	0.790	1.133

Table 4 gives the bulk modulus, shear modulus, hardness, universal elastic anisotropy index and ratio of G to B.

According to the Pugh criterion, when G/B<0.57 [31], the material is ductile; when G/B>0.57, the material appears brittle, and the larger the value, the more obvious the brittleness. We can see from Table 4 that the values of G/B after doping all become smaller and the brittleness is improved. With the increase of doping ratio, the brittleness is improved more obviously.

In order to improve the mechanical properties and extend the durability of the contact material, it requires further research on the structure of materials. It has been proved that the possibility of microcracks in the material is related to the elastic anisotropy index of the crystal. The universal elastic anisotropy index of the crystal reflects the difference of bonding strength in different directions, and is closely related to the induction of microcracks in the material. The universal elastic anisotropy index is usually the decisive factor for cracks. Table 4 shows that the A^U value after doping is smaller than that of SnO_2, and the smaller the doping ratio, the smaller the universal elastic anisotropy index, and the less likely it is to form microcracks.

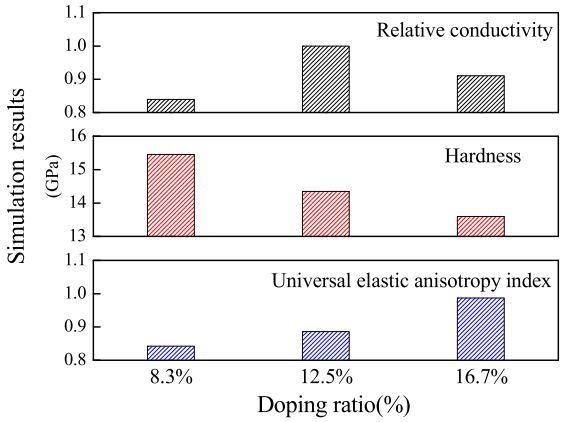

FIGURE 4. Simulation results of the relative conductivity, hardness and universal elastic anisotropy index of three doping ratios.

A polyline comparison chart of the relative conductivity, hardness and elastic anisotropy index of the three doping ratios is shown in Fig. 4.

When characterizing the properties of different ratio Gd doped $AgSnO_2$ contact materials, the effects of conductivity, hardness and universal elastic anisotropy index are simultaneously considered. Fig. 4 shows that the three performance parameters obtained by the same doping ratio are not the best and the worst at the same time. If subjectively describes that one is good and the other is slightly worse, it may not be convincing. At this time, a comprehensive performance evaluation system becomes extremely important.

IV. EVALUATION

The comprehensive evaluation can calculate synthesized indicators according to the multi indicators, simplify the multi-dimensional space problems into one-dimensional space problem, and rank the evaluation objects according to the values of the comprehensive indicators.

A. CONSTRUCTION OF EVALUATION MODEL

Technique for Order Preference by Similarity to Ideal Solution (TOPSIS) model is called approximation to ideal solution ranking method, which is a decision technology for multi objective decision analysis of finite schemes in system engineering, and a distance comprehensive evaluation method [32].

Combining the objectivity of entropy weight with TOPSIS model that can make full use of original data and rank the advantages and disadvantages of each scheme to be evaluated, and realizing the natural conversion from qualitative analysis to quantitative value. The construction steps are as follows.

The original decision matrix (R) consisting of m evaluation schemes to be evaluated and n evaluation indicators.

$$R = \begin{bmatrix} a_{11} & a_{12} & \cdots & a_{1j} \\ a_{21} & a_{22} & \cdots & a_{2j} \\ \vdots & \vdots & \ddots & \vdots \\ a_{i1} & a_{i2} & \cdots & a_{ij} \end{bmatrix}$$

Because the units of indicators are different, it is necessary to use the vector normalization method to deal with the corresponding data matrix to obtain the standardized decision matrix (X) The Equation is as shown in (17).

$$x_{ij} = \frac{a_{ij}}{\sqrt{\sum_{i=1}^{m} a_{ij}^2}} \tag{17}$$

B. CONSTRUCTION OF EVALUATION INDEX WEIGHT

The entropy weight is an objective weighting method. The change of the entropy value reflects the change of the disorder degree of the original data. The weight is completely determined according to the degree of data dispersion between evaluation indicators, starting from the data itself, which can effectively eliminate the human interference factors and make the final evaluation result objective [33].

The steps of entropy weight method are as follows.

1) The calculation of entropy weight is performed on the standardized decision matrix obtained by normalizing the original data.

The entropy values of the evaluation indicators determined by the n indicators are:

$$E_j = -\frac{1}{\ln m} \sum_{i=1}^{m} f_{ij} \ln f_{ij} \tag{18}$$

Among them, $f_{ij} = y_{ij} / \sum_{i=1}^{m} y_{ij}$,

$$y_{ij} = \begin{cases} \dfrac{a_{\max j} - a_{ij}}{a_{\max j} - a_{\min j}} \text{(The smaller the better)} \\ \dfrac{a_{ij} - a_{\min j}}{a_{\max j} - a_{\min j}} \text{(The bigger the better)} \end{cases}$$

When $y_{ij} = 0$, $\lim_{f_{ij} \to 0} f_{ij} \ln f_{ij} = 0$ is defined.

2) The entropy weight of evaluation indicators is:

$$W_j = \frac{1 - E_j}{\sum_{j=1}^{n} (1 - E_j)} \tag{19}$$

3) Construction of weighted standardized decision matrix

Multiply each column of the standardized decision matrix with the corresponding weight w_j to obtain the weighted standardized decision matrix (V). The Equation is defined as:

$$V = \begin{bmatrix} v_{11} & v_{12} & \cdots & v_{1j} \\ v_{21} & v_{22} & \cdots & v_{2j} \\ \vdots & \vdots & \ddots & \vdots \\ v_{i1} & v_{i2} & \cdots & v_{ij} \end{bmatrix} = X \times W \tag{20}$$

4) Determine positive and negative ideal solutions

The positive ideal solution V^+ and negative ideal solution V^- of the weighted standardized decision matrix are determined.

$$V^+ = \left\{ \left(\min v_{ij} \,|i = 1, 2, \ldots, m \right) \right\} \tag{21}$$

$$V^- = \left\{ \left(\max v_{ij} \,|i = 1, 2, \ldots, m \right) \right\} \tag{22}$$

5) Calculate the Euclidean distance

Calculating the Euclidean distance of each scheme to be evaluated with the best scheme (d_i^+), and with the worst scheme (d_i^-), respectively

$$d_i^+ = \sqrt{\sum_{j=1}^{n}(v_{ij} - v_j^+)^2} \tag{23}$$

$$d_i^- = \sqrt{\sum_{j=1}^{n}(v_{ij} - v_j^-)^2} \tag{24}$$

6) Calculate the closeness (c_i) of scheme to be evaluated with the best situation

The larger the value of c_i, the closer the scheme to be evaluated is to the positive ideal solution, and the better the scheme to be evaluated, Equation (25) is the closeness.

$$c_i = \frac{d_i^-}{d_i^- + d_i^+} \tag{25}$$

The data of the evaluation indexes of relative conductivity, hardness, and universal elastic anisotropy index are selected as the original data, and the data of different ratio of Gd doped SnO_2 are shown in Table 5.

TABLE 5. Original data for evaluation indicators.

Serial Number	Doping Ratio	σ	HV	A^U
I	16.7%	0.911	13.599	0.987
II	12.5%	1.000	14.351	0.886
III	8.3%	0.840	15.458	0.842

(17) is used to process the original data of Gd doped SnO_2 with different ratio to obtain the standardized decision matrix:

$$X = \begin{bmatrix} 0.572 & 0.542 & 0.629 \\ 0.628 & 0.572 & 0.564 \\ 0.528 & 0.616 & 0.534 \end{bmatrix}$$

Using (18) to normalize the original data, we get:

$$Y = \begin{bmatrix} 0.444 & 1 & 0 \\ 1 & 0.602 & 0.697 \\ 0 & 0 & 1 \end{bmatrix}$$

The entropy value of each evaluation indicators is calculated by (19):

$$E = \begin{bmatrix} 0.562 & 0.603 & 0.616 \end{bmatrix}$$

The entropy weight of each evaluation indicators calculated by using (20) is:

$$W = \begin{bmatrix} 0.359 & 0.326 & 0.315 \end{bmatrix}$$

Multiply each column of the standardized decision matrix with the corresponding weight w_j to obtain the weighted standardized decision matrix.

$$V = \begin{bmatrix} 0.205 & 0.177 & 0.198 \\ 0.225 & 0.187 & 0.178 \\ 0.190 & 0.201 & 0.168 \end{bmatrix}$$

The positive ideal and negative ideal solutions can be determined from (21) and (22) are:

$$V^+ = \begin{bmatrix} 0.225 & 0.177 & 0.168 \end{bmatrix}$$
$$V^- = \begin{bmatrix} 0.190 & 0.201 & 0.198 \end{bmatrix}$$

From (23) and (24), the Euclidean distances between the pairing schemes and the ideal and negative ideal solutions can be obtained.

$$d_{\mathrm{I}}^+ = 0.036 \quad d_{\mathrm{II}}^+ = 0.014 \quad d_{\mathrm{III}}^+ = 0.042$$
$$d_{\mathrm{I}}^- = 0.028 \quad d_{\mathrm{II}}^- = 0.043 \quad d_{\mathrm{III}}^- = 0.030$$

Combining the Euclidean distance of each scheme with the ideal solution and the negative ideal solution from (25), we can get the closeness of each scheme to the optimal scheme.

$$c_{\mathrm{I}} = 0.439 \quad c_{\mathrm{II}} = 0.752 \quad c_{\mathrm{III}} = 0.414$$

We can see from the closeness of different ratio of Gd doped SnO_2 when the doping ratio of 12.5% is the closest to the optimal scheme, followed by 16.7%.

V. EXPERIMENT

A. SOL-GEL METHOD

The traditional powder metallurgy method can only mechanically mix the doped element powder, SnO_2 powder and silver powder, and it is difficult to mix the doped element into the SnO_2 lattice, which is difficult to correspond to the theoretical model in this paper. In order to correspond to the SnO_2 model with different doping ratio obtained by the atom substitution method and to make the experimental results more convincing and comparable, Gd doped SnO_2 powders with different ratio are prepared by sol-gel method.

The precursors used in sol-gel method are alkoxides or inorganic salts. Because the price of alkoxide is expensive, the inorganic salt (MCl_n) is used as the precursor. Ammonia is added dropwise to the solution to promote the hydrolysis reaction and gradually form a chemical precipitation. The main reaction during the hydrolysis process is: $M^{m+}+mH_2O \rightarrow M(OH)_m\downarrow+mH^+$ [34]. The gel is obtained by sufficiently washing, and filtering the precipitate. The main reaction is: $M(OH)_m\downarrow \rightarrow MO_{m/2}+m/2H_2O$ [35]. Finally, the colloid is dried and sintered to prepare the required powder.

The sol-gel method is used to prepare Gd doped SnO_2 powder, and the main ingredients are shown in Table 6.

TABLE 6. Atomic and mass ratio of main materials.

$SnCl_4 \cdot 5H_2O$: $GdCl_3 \cdot 6H_2O$	16.7%	12.5%	8.3%
Atomic Ratio	83.3:16.7	87.5:12.5	91.7:8.3
Mass Ratio	0.99:0.21	1.04:0.16	1.09:0.11

B. X-RAY DIFFRACTION TEST

X-ray diffraction (XRD) test is performed to verify that the theoretical model matches the experiment. Each crystal has its own unique XRD diffraction peak. Whether the doped elements enter into the SnO_2 crystal can be judged by the change of the main diffraction peak position of the XRD pattern.

XRD test is carried out by a Bruker D8 DISCOVER. The test adopts a continuous scanning mode. The X-ray generator is a Cu target K_α ray, λ is 0.15405nm, the scanning range is 10∼90°, and the scanning speed is 12°/min. Fig. 5(a) is the X-ray diffraction test of SnO_2 powder, and (b) is the SnO_2 powder with Gd doping ratio of 16.7%.

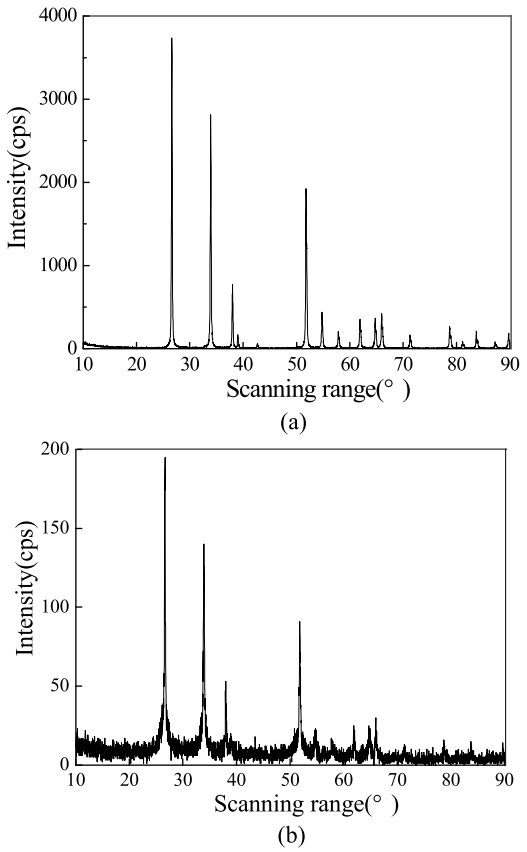

FIGURE 5. X-ray diffraction test (a) SnO_2 powder (b) 16.7%-Gd doped SnO_2 powder.

The peak position of the diffraction peak of the Gd doped SnO_2 powder is basically the same as that of SnO_2, that is, after Gd doped, it shows that the characteristic diffraction peaks of the metal oxide or metal element do not appear in the XRD pattern, the crystal structure of SnO_2 is not changed, indicating that the material prepared by sol-gel process better achieves the gap doping and is consistent with the theoretical model. Moreover, the diffraction peak of Gd doped $SnO_2$is wider than that of SnO_2 and the intensity decreases, which indicates that the particles obtained by the sol-gel method are finer and the crystallinity of grains becomes weaker.

C. POWDER METALLURGY

First, Gd doped SnO_2 powder is prepared by sol-gel method, and then 1.2g of Gd doped SnO_2 powder and 8.8g of Ag powder are weighed and mixed by a high energy ball mill. A series of processes such as initial pressure, initial sintering, repressing, reburning, polishing and cutting to obtain Gd doped $AgSnO_2$ contact material. Finally, the hardness, electrical conductivity, contact resistance and arc energy are measured, and surface morphology of the contacts after electrical contact experiments are given.

D. ELECTRICAL PERFORMANCE

The experiment uses electrical contact material testing equipment JF04C for electrical contact performance. The JF04C test system is mainly composed of a power cabinet, a computer, a test cabinet, and a test bench. Before the experiment, the cut sample must be placed in the fixture on the test bench, and the test parameters (such as closing pressure, operating frequency) must be set on the computer to start the experiment and collect data.

This experiment is a simulated electrical contact, using a DC resistive load. The voltage of system is set to ±40V, the contact opening distance is 10mm, the contact pressure is 86cN. The simulation test of the contact work under the condition of direct current 13A. There is no arc extinguishing device installed in the test equipment, and direct current is used in the test process, and no arc over zero point, so the contact ablation is more serious than the actual application, and the electrical life of the sample is relatively short. Research shows that the data collected during the 25,000 opening and closing experiments under the conditions set can reflect the performance of the contact material. In addition, considering the cost of the material and the test cycle, the number of actions selected is 25000. The arc energy, average arc energy, contact resistance and average contact resistance of $AgSnO_2$ and $AgSnO_2$ contact materials with Gd doped are shown in Table 7.

Sigmas cope SMP10 metal conductivity tester is used to measure the sample conductivity. The principle of metal conductivity tester is electromagnetic induction, and indirectly assess the conductivity of materials.

The measurement frequency is selected as 60KHZ. The test probe ES40 of the handheld eddy current non-ferrous metal conductivity tester is used for experiment. The probe is placed on the metal surface to be tested directly. The data processing uses a single chip microcomputer and is equipped with

TABLE 7. Parameters for electrical measurement.

Doping Ratio	16.7%	12.5%	8.3%	0
Arc Energy(mJ)	169.1~190.9	167.9~181.8	170.9~198.6	159.0~235.3
Average Arc Energy(mJ)	175.6	175.5	180.1	192.9
Contact Resistance (mΩ)	0.96~4.26	0.35~1.52	0.49~5.06	0.35~8.93
Average Contact Resistance (mΩ)	1.66	0.64	1.71	1.83
Conductivity (MS/m)	31.94	33.37	28.78	26.44

a temperature compensation device, which automatically calibrates the conductivity value to make the test environment more stable and the measured data is relatively accurate. Five measurements are performed on each sample and the average value is determined, as shown in Table 7.

Table 7 shows that the arc energy and contact resistance of the Gd doped $AgSnO_2$ contact material present the same change trend. The average arc energy and the average contact resistance of the doped contact material both become lower than that of $AgSnO_2$ contact material, and the minimum and maximum values of arc energy and contact resistance are reduced, and the range of variation is also narrowed.

The measured conductivity is also consistent with the relative conductivity, which proves that the simulation is correct.

Fig. 6 shows the relationship between the arc energy of the contact material and the number of actions when the contact is measured for the arc energy once every 100 times, and 25000 actions contact movement. Among them, (a) is the $AgSnO_2$ contact material, (b), (c), and (d) are $AgSnO_2$ contact materials with a doping ratio of 16.7%, 12.5%, and 8.3, respectively.

Because the rare earth element easily loses the outermost electrons and forms a stable structure with high melting point, it is not easy to decompose under the action of the arc, but gathers on the surface of contact, thereby reducing the ablation of the contact by the arc and the arc energy. Fig. 6 shows the arc energy after doping is reduced, the fluctuations become smaller, that is, and the arc energy becomes smaller and stable. When the doping ratio is 12.5%, The arc energy is smaller and more stable, followed by the doping ratio of 16.7%.

E. MORPHOLOGY ANALYSIS OF ARC EROSION

Scanning electron microscopy (SEM) is used to analyze the surface morphology of $AgSnO_2$ contact material. Fig. 7 shows the surface morphology after 25,000 times electrical contact performance tests of the contact material.

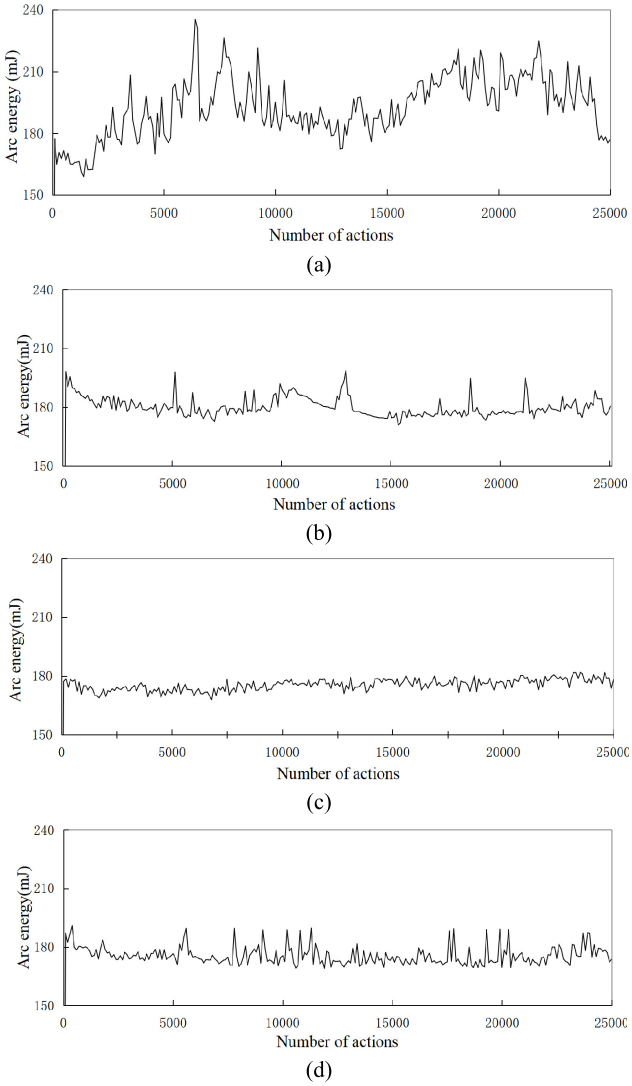

FIGURE 6. Arc energy (a) SnO_2 (b) 16.7%-Gd doped SnO_2 (c) 12.5%-Gd doped SnO_2 (d) 8.3%-Gd doped SnO_2.

(a) is the $AgSnO_2$ contact material. (b), (c), and (d) are the $AgSnO_2$ contact materials with doping ratio of 16.7%, 12.5%, and 8.3, respectively.

It can be seen from the surface morphology of $AgSnO_2$ in Fig. 7(a) that there are holes and ablation pits on the contact surface, as well as a large number of SnO_2 aggregates, making the contact surface rough. Moreover, the poor conductivity of SnO_2 will deteriorate the contact characteristics, increasing the contact resistance and releasing more Joule heat.

After doping, the contact surface is smooth and dense, without large area of ablation pit. indicating that the Gd doped can be dispersed in the silver matrix to avoid agglomeration. Combined with contact resistance, arc energy and surface erosion morphology, the doped contact has low and stable contact resistance and low Joule heat. Secondly, the arc energy of the contact is small, the stability is good, the arc action time is short, and the temperature rise of the contact surface is relatively slow. Moreover, 12.5% doping is the best,

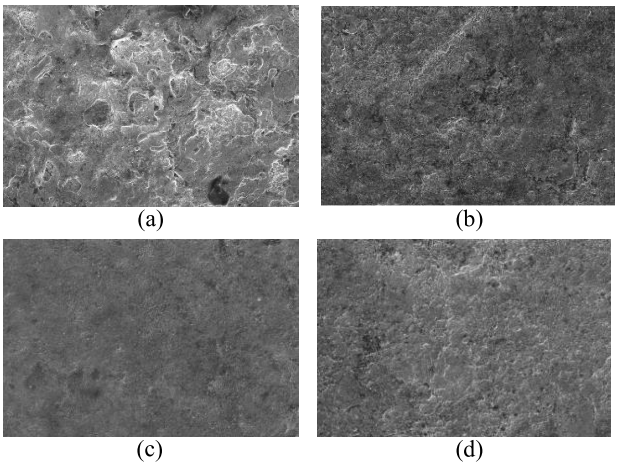

FIGURE 7. Surface morphology (a) SnO_2 (b) 16.7%-Gd doped SnO_2 (c) 12.5%-Gd doped SnO_2 (d) 8.3%-Gd doped SnO_2.

followed by 16.7%. This is consistent with the better doped element ranking of the evaluation results.

F. HARDNESS

HXD-1000TM digital microhardness tester is used to measure the hardness of the contact material. Firstly, the test pressure is selected, and turn the diamond indenter to the surface of the sample to be tested. After holding for a few seconds, using a microscope to find and observe the diamond indentation on the surface of the sample. Then, we adjust the position of the raster and place it on the two diagonals of the diamond on both sides, measuring the length of the diagonal. Finally, reading the hardness value. To improve the credibility of the calculation results, five positions are selected for each sample, and then take the average value of five groups of data.

TABLE 8. Hardness.

Doping Ratio	Hardness (HV)
16.7%	85.2
12.5%	89.6
8.3%	92.0
0	117.1

Compared with the hardness calculated by simulation in Table 8, it is found that hardness is reduced with the increase of doping ratio and the order of the theoretical and experimental hardness are the same.

VI. CONCLUSION

Three kinds (8.3%, 12.5%, 16.7%) of rare earth elements Gd doped SnO_2 are simulated based on the first principle of density functional theory.

The relative conductivity of different doping ratio can be obtained by integrating the density of states and the two times derivative of energy band. The relative conductivity is the best when the doping ratio is 12.5%, followed by 16.7%.

Then calculate the elastic constant of the simulation model. As the doping ratio increases, the smaller the hardness, the larger the probability of microcracks.

Relative conductivity, hardness and universal elastic anisotropy index are selected as the evaluation indicators of the comprehensive evaluation model of Technique for Order Preference by Similarity to Ideal Solution (TOPSIS) with entropy weight. When the doping ratio of 12.5%, the closeness of Gd doped SnO_2 is the closest to the optimal scheme, that is, the comprehensive performance with the doping ratio of 12.5% is the best.

Finally, the experiments are used to verify the results. The average arc energy and the average contact resistance of the Gd doped $AgSnO_2$ contact materials are reduced, and the measured conductivity and hardness are also consistent with the theoretical results.

It provides a new simulation and evaluation method for screening the doping ratios and elements in the future to obtain $AgSnO_2$ contact materials with the best performance.

REFERENCES

[1] X. Zhang, W. Ren, Z. Zheng, and S. Wang, "Effect of electrical load on contact welding failure of silver tin oxide material used in DC electromechanical relays," *IEEE Access*, vol. 7, pp. 133079–133089, 2019.

[2] F. Pons and M. Cherkaoui, "An electrical arc erosion model valid for high current: Vaporization and splash erosion," in *Proc. 54th IEEE Holm Conf. Electr. Contacts*, Orlando, FL, USA, Oct. 2008, pp. 9–14.

[3] C. H. Leung, "Molded case circuit breaker electric contact erosion and design for reliability," in *Proc. 6th ICRE Conf. Elect. Contacts*, Wenzhou, China, 2017, pp. 6–10.

[4] E. George and M. Pecht, "RoHS compliance in safety and reliability critical electronics," *Microelectron. Rel.*, vol. 65, no. 1, pp. 1–7, Oct. 2016.

[5] H. S. Lee, H. W. Shin, T. K. Jung, T. B. Kim, and M. H. Lee, "Microstructure and hardness property of internally oxided AgCdO alloy," *Appl. Mech. Mater.*, vols. 152–154, no. 1, pp. 440–443, Jan. 2012.

[6] L. Doublet, N. B. Jemaa, S. Rivoirard, C. Bourda, E. Carvou, D. Sallais, D. Givord, and P. Ramoni, "New contact material for reduction of arc duration for DC application," *Eur. Phys. J. Appl. Phys.*, vol. 50, no. 1, p. 12901, Apr. 2010.

[7] L. Morin, N. B. Jemaa, D. Jeannot, J. Pinard, and L. Nedelec, "Contacts materials performances under break arc in automotive applications," *IEEE Trans. Compon. Packag. Technol.*, vol. 23, no. 2, pp. 367–375, Jun. 2000.

[8] E. Brisson, P. Carre, H. Desplats, P. Rogeon, V. Keryvin, and A. Bonhomme, "Effective thermal and electrical conductivities of $AgSnO_2$ during sintering. Part I: Experimental characterization and mechanisms," *Metall. Mater. Trans. A*, vol. 47, no. 12, pp. 6304–6318, Dec. 2016.

[9] Z. K. Chen and G. J. Witter, "A study of dynamic welding of electrical contacts with emphasis on the effects of oxide content for silver tin indium oxide contacts," in *Proc. 56th IEEE Holm Conf. Electr. Contacts*, Charleston, SC, USA, Oct. 2010, pp. 121–126.

[10] H. Cinaroglu, V. Behrens, and T. Honig, "Application of a new Ag/SnO_2 contact material in AC-contactors," in *Proc. 63rd IEEE Holm Conf. Electr. Contacts*, Denver, CO, USA, Oct. 2017, pp. 215–220.

[11] F. Chong, J. Fengyang, and W. Junbo, "Effect of La doping on arc erosion products of nanocomposite $AgSnO_2$ contact alloys," *Trans. China Electrotech. Soc.*, vol. 25, no. 5, pp. 44–47, May 2010.

[12] H. Wang, J. Wang, J. Du, and F. Meng, "Influence of rare Earth on the wetting ability of $AgSnO_2$ contact material," *Rare Metal Mater. Eng.*, vol. 43, no. 8, pp. 1846–1849, Aug. 2014.

[13] Z. Ying, W. Jingqin, and K. Huiling, "Study on electrical properties of $AgSnO_2$ contact materials doped with rare-earth La, Ce, and Y," *IEEE Trans. Compon., Packag., Manuf. Technol.*, vol. 9, no. 5, pp. 864–870, May 2019.

[14] K. G. Godinho, A. Walsh, and G. W. Watson, "Energetic and electronic structure analysis of intrinsic defects in SnO_2," *J. Phys. Chem. C*, vol. 113, no. 1, pp. 439–448, Jan. 2009.
[15] Y. Chen, Y. X. Lu, Y. W. Xie, and Q. M. Zhang, "Supply chain interface risk assessment based on entropy weight improvement TOPSIS model," *China Storage Transp.*, vol. 10, no. 1, pp. 113–117, Jan. 2018.
[16] T. T. Zhang, "First-principles calculation of the electronic structure of doped zinc oxide," M.S. thesis, Dept. Softw. Eng., Huazhong Univ. Sci. Technol., Wuhan, China, 2009.
[17] M. D. Segall, P. J. D. Lindan, M. J. Probert, C. J. Pickard, S. J. Clark, and M. C. Payne, "First-principles simulation: Ideas, illustrations and the CASTEP code," *J. Phys*, vol. 14, no. 11, pp. 2717–2744, Mar. 2002.
[18] M. Hu, Z. Chen, C. Li, F. Li, J. Wang, and L. Jiao, "Elasticity, hardness and anisotropies of bc-B_nCN (n=1, 2, 4)," *Scientia Sinica Phys., Mechanica Astronomica*, vol. 46, no. 6, pp. 1–13, Apr. 2016.
[19] L. T. Shan, D. C. Ba, Y. H. Lin, and J. C. Li, "Study on the structure and optical properties of Ce-doped SnO_2 materials," *Vacuum*, vol. 51, no. 1, pp. 25–28, Jan. 2014.
[20] J. G. Jia, X. J. Xie, Z. H. Liang, X. C. Zhang, C. M. Fan, and P. D. Han, "First-principles study of Ti-doped SnO_2 semiconductor solid solutions," *Chem. J.*, vol. 33, no. 5, pp. 1050–1056, Apr. 2012.
[21] W. J. Wang, Z. L. Liu, Q. Xi, Z. D. Zhang, and Q. D. Wang, "First-principles study on the stability and electronic structure of Mg-Er intermetallic compounds," *J. Nonferrous Met.*, vol. 24, no. 2, pp. 343–350, Feb. 2014.
[22] J. Q. He, "First-principles study of the structure and properties of rare earth-doped NiAl intermetallic compounds," Ph.D. dissertation, Dept. Mater. Eng., Harbin Inst. Technol., Harbin, China, Tech. Rep., 2013.
[23] Z. B. Li, G. S. Zhang, and Y. Qi, "Research on the resistance to dynamic fusion welding of electrical contact materials and their different matings," *Trans. China Electrotech. Soc.*, vol. 3, no. 1, pp. 61–64, Jan. 1993.
[24] E. K. Liu, B. S. Zhu, and J. S. Luo, *Semiconductor Physics*, 6th ed. Beijing, China: Publishing House of Electronics Industry, 2003, pp. 111–129.
[25] W. Voigt, *Lehrbuch Der Kristallphysik*. New York, NY, USA: Macmillan, 1908, p. 962.
[26] A. Reuss, "Calculation of the flow limits of mixed crystals on the basis of the plasticity of monocrystals," *Z Angew Math. Mech.*, vol. 9, no. 1929, pp. 49–58, May 1929.
[27] R. Hill, "The elastic behaviour of a crystalline aggregate," *Proc. Phys. Soc. A*, vol. 65, no. 5, pp. 349–354, May 1952.
[28] S. I. Ranganathan and M. Ostoja-Starzewski, "Universal elastic anisotropy index," *Phys. Rev. Lett.*, vol. 101, no. 5, pp. 349–354, Aug. 2008.
[29] X.-Q. Chen, H. Niu, D. Li, and Y. Li, "Modeling hardness of polycrystalline materials and bulk metallic glasses," *Intermetallics*, vol. 19, no. 9, pp. 1275–1281, Sep. 2011.
[30] Y. Tian, B. Xu, and Z. Zhao, "Microscopic theory of hardness and design of novel superhard crystals," *Int. J. Refractory Met. Hard Mater.*, vol. 33, no. 6, pp. 93–106, Jul. 2012.
[31] S. F. Pugh, "Relations between the elastic moduli and the plastic properties of polycrystalline pure metals," *J. Sci.*, vol. 4, no. 5, pp. 823–843, Mar. 1954.
[32] X. Li, K. Wang, L. Liu, J. Xin, H. Yang, and C. Gao, "Application of the entropy weight and TOPSIS method in safety evaluation of coal mines," *Procedia Eng.*, vol. 26, pp. 2085–2091, Dec. 2011.
[33] G. Xin, C. Yang, and Q. Yang, "Post-evaluation of well-facilitied capital farmland construction based on entropy weight method and improved TOPSIS model," *Trans. Chin. Soc. Agricult. Eng.*, vol. 33, no. 1, pp. 238–249, Jan. 2017.
[34] Q. H. Gu, "Preparation of tin dioxide gas-sensitive film by sol-gel method," M.S. thesis, Dept. Integr. Circuit Eng., Huazhong Univ. Sci. Technol., Wuhan, China, Tech. Rep., 2013.
[35] C. Delmas, M. Maccario, L. Croguennec, F. Le Cras, and F. Weill, "Lithium deintercalation in $LiFePO_4$ nanoparticles via a domino-cascade model," *Nature Mater.*, vol. 7, no. 8, pp. 665–671, Aug. 2008.

YING ZHANG was born in Baoding, Hebei, in 1993. She received the M.S. degree in electrical engineering from the Hebei University of Technology, where she is currently pursuing the Ph.D. degree.

JINGQIN WANG was born in Hengshui, Hebei, in 1964. She received the B.S., M.S., and Ph.D. degrees in electrical engineering from the Hebei University of Technology, Tianjin, China, in 1984, 1986, and 1997, respectively.

Since 1998, she has been a Professor. She became a Doctoral Tutor with the Electrical Engineering College, Hebei University of Technology, in 2003. She currently holds 21 patents. She has written more than 110 journal articles. She is also a coauthor of the book titled as *Reliability Basic Theories and Applications in Electrical Apparatus* (Bloomington, USA: iUniverse, 2012), and a national standard *GB/Z 22203-2016 Reliability test method of circuit-breakers for overcurrent protection for household and similar installation* (Beijing, China: China Standard Press, 2016). Her research interests include reliability theories, electrical contact phenomenon, environmental effect on electrical contact, electrical contact material, and contact failure simulation and life prediction.

Prof. Wang was a recipient of the National Science and Technology Progress Award, in 2000, 2002, and 2008, and the Science and Technology Progress Award of Hebei Province, in 1991, 2005, and 2013. She is also the Secretary General of the Electrical Products Reliability Association of China Electro Technical Society (CES). She is also the Deputy Director of the Institute of Electrical Appliances of Hebei University of Technology, and an Expert on special allowances of the State Council, a national candidate for hundreds of millions of the talents project of the new century, and an outstanding expert of Hebei Province. She is also the Vice Chairman and a member of the Arc-electricity Contact Committee of China Electrotechnical Society and a member of the Low-voltage Electrical Appliances Committee of China Electrotechnical Society.

GUANGZHI ZHANG, photograph and biography not available at the time of publication.

ZHIZHOU BAO, photograph and biography not available at the time of publication.